PROBLEMS OF WET UNDERWATER WELDING OF DUPLEX STEELS

S.Yu. Maksymov, A.A. Radzievska, D.V. Vasyliev and **G.V. Fadeeva**

E.O. Paton Electric Welding Institute of the NAS of Ukraine

11 Kazymyr Malevych Str., 03150, Kyiv, Ukraine. E-mail: office@paton.kiev.ua

The article considers the problem of welding duplex steels: state-of-the-art of the problem and prospects for further development. Welds made in air and under water using coated electrodes, are characterized by a similar structure and properties. Intensive cooling provided by the water environment does not increase the content of ferrite in the weld and HAZ as compared to its content in the joints made in the air. Butt joints produced under water at an unstable arc burning are characterized by a tendency to cold crack formation in the weld metal, but in the HAZ cracks were not detected. In the article the analysis of hardness distribution in the studied joints was presented, which did not reveal significant differences between the values determined in the welds made in air and in water. The size of austenitic phases in dry welding was larger than in wet welding under the same conditions of heat input. In wet welding, the share of γ-phase increased significantly at increase in input energy from 27.31 to 39.46 % for the weld center and from 35.01 to 44.9 % for the weld metal adjacent to the fusion line. All the studied variants of chemical composition of the weld metal were insensitive to local corrosion due to high values of PREN. The weld metal adjacent to the fusion line showed optimal resistance to local corrosion, and the weld metal also showed better resistance to local corrosion than did the heat-affected-zone. 17 Ref., 1 Table, 8 Figures.

K e y w o r d s : duplex steels, underwater welding, welded joint, formation, structure, corrosion, service properties, welding consumables

From the start of 1900s, duplex and superduplex stainless steels have an important role in oil and gas industry, in transportation, construction and processing industry [1]. By now the sphere of their application expanded to metal structures that operate in water environment, in particular, at construction of navy and nuclear power units, pipelines for sulphur trioxide, oil and sea water, due to a favourable combination of high mechanical strength and general and local corrosion resistance and cracking resistance, caused by interaction of stresses and hydrogen, the source of which is the acid environment of liquid hydrocarbons, as well as lower cost due to lower nickel content [2].

Modern duplex stainless steels usually contain 4.5–7.5 % nickel and 20–25 % chromium at a low level of carbon and have a two-phase ferrite-austenite microstructure. As one can see from the diagram of phase transformation of Fe–Cr–Ni system [3] (Figure 1), when Cr/Ni equivalent ratios are higher than 1.75, just the ferrite phase evolves from the liquid up to complete crystallization. During the further cooling process ferrite partially transforms into austenite, when the temperature drops to that of δ→γ transformation, which is determined by the chemical composition. During ferrite transformation into austenite with cooling, the austenite morphology can be consistently manifested in the form of grain-boundary amorphous structures, Widmanstatten

side plates or intragranular side plates, acicular, as well as fine intragranular precipitates [4]. With the start of transformation, austenite first appears on the boundary of the grains due to its maximum free energy. Transformation of intragranular austenite requires the greatest driving force, and takes place at the lowest possible temperature. The temperature of transformation of austenite of Widmanstatten side plate is between two of the above-mentioned temperatures. The degree of transformation and
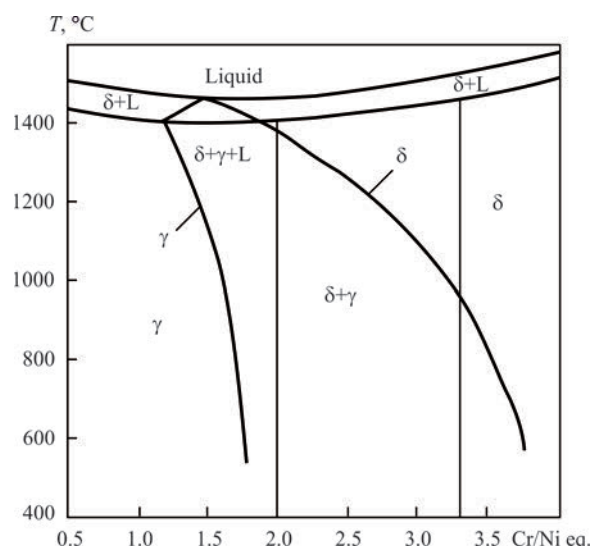

Figure 1. Diagram of pseudobinary phase transformation of Fe–Cr–Ni system [3]

S.Yu. Maksymov — https://orcid.org/0000-0002-5788-0753

final morphology of austenite are determined by chemical composition and cooling rate. The higher the content of austenite stabilizers, the greater is the degree of its transformation. The higher the cooling rate, the more acicular and fine precipitates are present in ferrite.

Mechanical properties and corrosion resistance of duplex steel welded joints depend on ferrite and austenite fraction in the structure, morphology and size of ferrite and austenite grains, type, morphology and distribution of intermetallic phases, which can precipitate from ferrite. Standard duplex and superduplex steels cover a whole range of microstructures, the properties of these alloys depend mainly on the balance of the two phases — ferrite and austenite. Any form of heat treatment, including thermal cycles of welding, influences the morphology of these steels, and, consequently, the mechanical and corrosion properties of the HAZ in welded joints [5]. So, at heating from approximately 600 up to 1000 °C, the superduplex stainless steels are prone to formation of intermetallic phases (for instance, σ-phase, χ-phase and R-phase) [6]. Reheating can also cause formation of secondary austenite and nitride precipitation. Presence of these phases considerably impairs the corrosion resistance and impact toughness.

The value of heat input and cooling rate have an essential influence on the microstructure and secondary phase formation in the HAZ. During welding, the HAZ is brought to a temperature, at which the material is practically completely ferritic. Austenite reformation starts at cooling. The degree of ferrite transformation into austenite depends on the steel composition and welding conditions. A higher content of nickel and nitrogen and slower cooling facilitate this transformation. At rapid cooling a high content of ferrite can be recorded in the HAZ, resulting in lowering of the joint strength and corrosion resistance. Ferrite content in the metal of the weld and HAZ should be within 25–70 %, so as to ensure optimum mechanical properties and corrosion resistance [7]. In order to achieve the required balanced microstructure, it is necessary to strictly control the filler metal composition and cooling rate. In the opinion of the authors of work [8], the filler metal composition has a stronger influence on the final ratio of ferrite/austenite than does the

Figure 2. Cross-section of an underwater weld [11]

cooling rate. Cold cracking susceptibility in the welded joints of duplex steels depends on ferrite content in their structure, heat input and hydrogen content in the shielding gas. It was noted that it becomes higher, if the ferrite content in the weld is more than 50 %. On the other hand, hydrogen addition to the shielding gas (Ar) led to reduction of cracking. The shape of edge preparation can also promote cold cracking due to unfavourable distribution of residual stresses after welding [9, 10].

Despite the broad application of duplex steels, the effect of water environment on the structure and properties of welded joints is little studied so far. There are no results of extensive research or reports on duplex steels behaviour at underwater welding and properties of the produced joints. The most unfavourable factors for underwater welding of duplex steel are believed to be increased cooling rate and hydrostatic pressure, and there also exists the risk of increased content of hydrogen in the ferritic phase [11, 12]. Here, most of the problems are associated with the HAZ and not with the weld.

At wet welding, the factors affecting the welding quality, are more complex than at dry welding, and the welding process is also more complicated. Most of the accessible results of the conducted experiments have been obtained at application of manual welding with industrial electrode materials, used in air, as specialized electrode materials for wet underwater welding of duplex steels have not been developed so far [13]. Here, the susceptibility to formation of cold cracks and pores, influence of the thermal cycle of welding directly in the water environment on the structure and properties of weld metal were assessed.

So, works [12, 14] give the results of determination of cold cracking resistance of 2205 UNS-S31803 stainless steel, using Tekken sample (1.4462). Welding was performed with Bohler FOX CN 22/9N (EN 1600 – E 22 9 3 N L R 3 2) electrodes of 4 mm diameter at the depth of 0.5 m. Tested samples had undercuts, lacks-of-fusion and incorrect shape. During underwater welding, it was noted that the arc was unstable, leading to sputtering, and uncontrolled increase of welding parameters that exceed the admissible heat input for duplex steels. The results of metallographic investigations revealed internal defects in the weld metal, namely pores and cracks, which formed in the root pass (Figure 2). HAZ was very narrow, and it could not be identified up to ×50 magnification. Base metal had a typical two-phase structure, which consists of a ferrite matrix (35–50 %) and austenite grains, arranged in bands; average ferrite content was equal to approximately 48 %. The weld structure consisted of precipitates of ferrite and acicular austenite normal to the fusion line (Figure 3, *a*); ferrite amount was in the range from 52 to 56 %. Difference in ferrite content between the base metal and weld can be the result
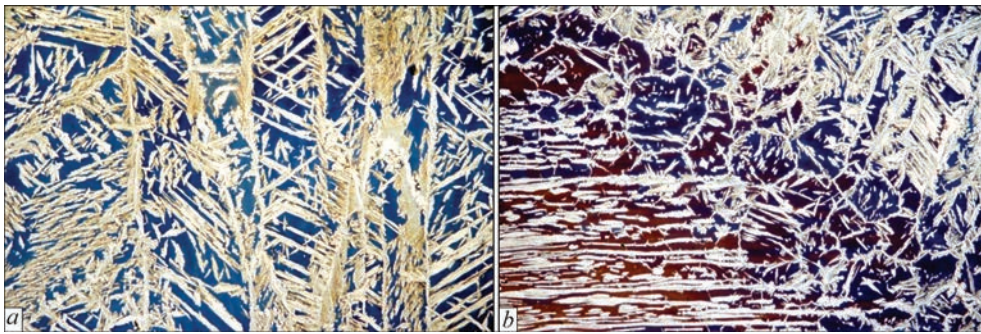
Figure 3. Microstructure (×100) of weld metal (*a*) and HAZ (*b*) [11]

of chemical composition of metal, deposited with FOX CN 22/9N electrodes, characterized by a higher content of nickel. The HAZ overheated zone (Figure 3, *b*) was characterized by a higher content of ferrite, which, however, did not exceed the limit value of 70 % and was in the range from 54 to 69 %, while the transition zone contained local purely ferritic bands.

Hardness measurement was conducted along a line located 2 mm below the control weld surface. Hardness distribution in the joint cross-section along the measurement line is characteristic for duplex steels: base metal hardness was not higher than HV 5–270, hardness of weld metal and HAZ was approximately the same, and did not exceed critical values. This leads to the conclusion that no processes of secondary phase precipitation occurred under the impact of the thermal cycle of welding. It should be added that accurate hardness measurement was made difficult by a very narrow HAZ.

Investigations of samples of S32101 steel joints, made with E2209-T0-4 flux-cored wire at the depths of 20 and 60 m with welding mode variation (see Table), demonstrated a certain correlation of porosity and weld metal microstructure [15, 16]. The appearance of the deposited metal and its X-ray pattern are given in Figure 4. Metal porosity in welds made at the depth of 60 m was 6 to 14 % that is almost two times higher than in welding at 20 m depth (Figure 5). The authors attribute it mainly to increase of hydrostatic pressure.

Comparing experiments No.1 with No.2 and No.5 with No.6 (see Table), it is easy to see that at both the water depths porosity increases with voltage rise, and increase rates are 21 and 67 %, respectively. Similarly, comparing No.3 with No.4 and No.6 with No.8, at

lowering of welding speed porosity decreases by 31 and 20 %, respectively. However, at lowering of welding current porosity increases by 46 % at 20 m depth, and decreases by 17 % at 60 m depth. Reduction of weld porosity at 60 m depth can be associated with a higher heat input that leaves more time for the dissolved gas to escape, despite the higher hydrostatic pressure. Changes in welding parameters which can give more time for hydrogen removal, promote reduction of porosity.

Cr/Ni ratio in the welding wire was equal to 2.56, and it corresponds to the type of completely ferritic crystallization. Initial solidification of the melt pool includes epitaxial growth of ferrite from base metal on the fusion boundary. The temperature gradient determines the initial direction of dendrite growth and promotes formation of coarse columnar ferritic structure.

Microstructure of the metal of welds made at the depth of 20 and 60 m, differs significantly by distribu-
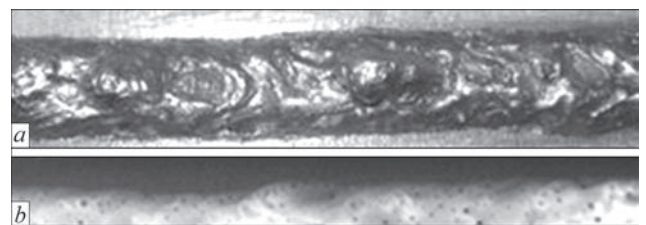

Figure 4. Appearance of the weld (*a*) and its X-ray pattern (*b*) [16]

Welding mode parameters [16]

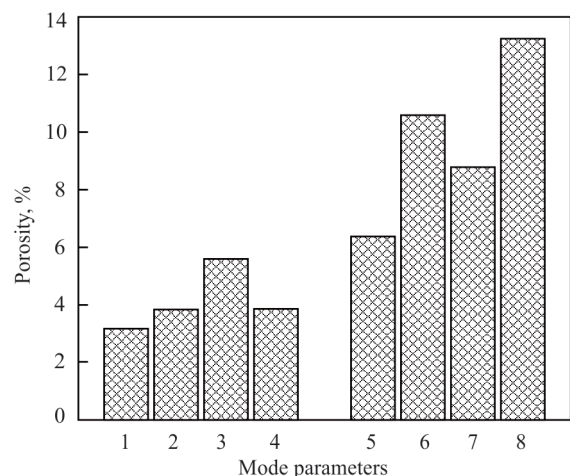| Number	U, V	I, A	V, mm/s	H, m	Q, kJ/mm	δ, %
1	27	275	8.5	20	874	3.16
2	33	275	8.5	20	1068	3.81
3	33	225	8.5	20	874	5.58
4	33	225	5.5	20	1350	3.86
5	27	275	5.5	60	1350	6.36
6	33	275	5.5	60	1650	10.59
7	33	225	5.5	60	1350	8.78
8	33	275	8.5	60	1068	13.23

Figure 5. Weld porosity at different welding parameters (1–8 — experiment numbers (see table); 1–4 — 20 m depth; 5–6 — 60 m depth [16]

tion and morphology of the austenitic phase. Any causes for reduction of the actually input amount of heat will stimulate initiation and growth of intragranular austenite due to relative increase of the cooling rate. Continuous network of austenite and fine particles develops in ferrite grains in the form of intragranular precipitates. The size of microstructural components of the weld metal can be reduced by increasing the welding speed.

When welding is performed with the same heat input, the microstructure and mechanical properties of the welds can differ. In other words, changing the input heat amount by changing the voltage or current can have different results. So, comparison of welds made in mode 1 and 3 (see Table) having the same heat input, shows that the high current promotes microstructure refinement. A similar result was obtained at welding in modes No.5 and No.7.

The authors explain the cause for the above phenomenon by a greater impact of the arc on the weld pool that causes a stronger convective motion, which leads to improvement of heat removal conditions.

The influence of welding parameters on the porosity and microstructure is of a complex and nonlinear nature. However, the diffusivity and solubility of hydrogen in ferrite and austenite differ significantly. The ferrite grain boundaries absorb hydrogen. Meanwhile, hydrogen atoms located on fine grain boundaries can diffuse easier, than those in larger grains. More over, increase of the heat input can extent the time of staying at a high temperature, and gas can easily leave the melt pool. As regards porosity and microstructure ratio, the welding parameters should be considered together.

Comparative studies of the structure of metal and HAZ at dry welding in the chamber and directly in the water environment [17] (Figure 6), showed that the width of the high-temperature region, which is heated above 1000 °C, somewhat decreases, and is equal to 30–70 μm. At the same time the austenite grain size also becomes smaller. The authors attribute it to shortening of the recrystallization time and increase of the amount of γ-phase, as well as limitations of diffusion of stabilizing elements from the weld metal. Farther from the fusion line, the volume fraction of austenite becomes smaller, more intensively at wet welding than at the dry process: from 35.01 to 25.39 % and from 51.61 to 32.29 %, respectively.

In the weld metal the previous transformation austenite (PTA) and grain boundary (GBA) austenite precipitated rapidly along the ferrite grain boundaries (Figure 6, weld section adjacent to the fusion line). A large amount of austenite precipitates in the form of Widmanstatten austenite (WA), which grows into the ferrite grains, and particles of intragranular austenite (IGA) of an acicular morphology are observed in the ferrite grains (Figure 6, weld metal in the center and near the fusion line). Compared to dry welding, the volume fraction of these structural components becomes smaller. A higher cooling rate shortened the transformation time. γ-stabilizers, such as N, Ni, and Mn had less time for diffusion that restrained the nucleation and growth of the austenite grains.

Microstructural studies of the HAZ high-temperature zone revealed appearance of pits on the boundaries of α–α and α–γ grains, as well as inside the ferrite grains that is indicative of precipitation of chromium-enriched nitrides in these areas after welding. The probability of their formation at wet welding becomes higher. With increase of the heat input, the volume fraction of chromium nitrides decreases as a result of cooling rate lowering.
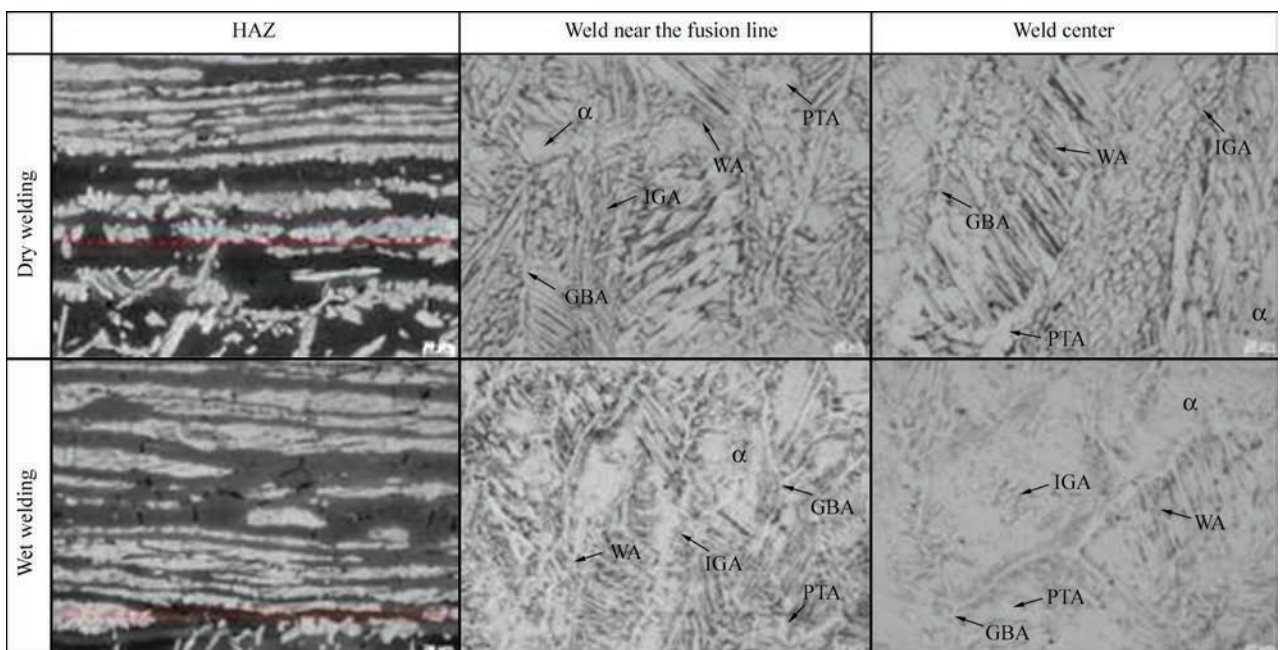

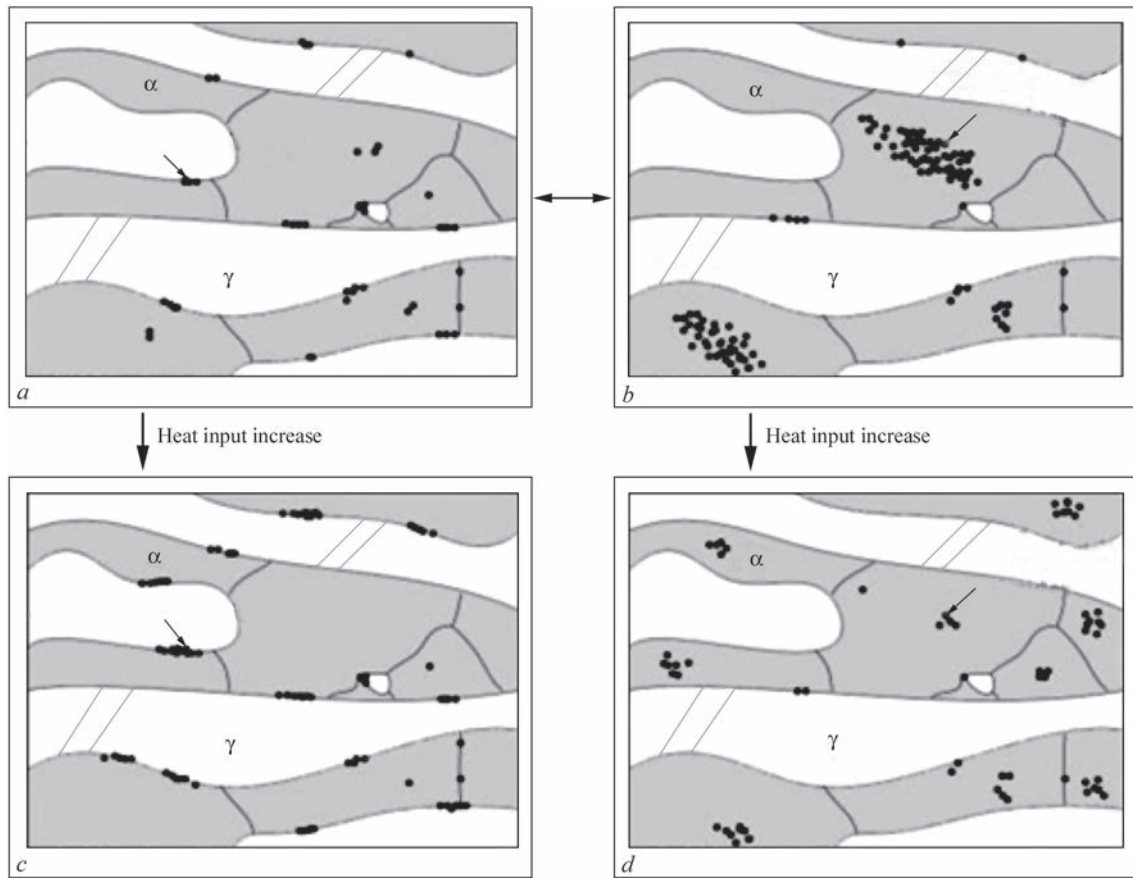**Figure 6.** Microstructure of welded joint zones [17]

Figure 7. Schematic diagrams of distribution of chromium-enriched nitrides in the HAZ low-temperature zone [17]. The arrows show chromium-enriched nitrides inside the α-phase and on α/γ boundary

A longer stay at increased temperature promotes nitride precipitation, which occurs on γ/α and α/α interface, due to a high coherence of these boundaries. In addition, a small amount of chromium nitrides appeared in α-phase. A large amount of heat allowed enough time for nitrogen atoms for diffusion that prevents oversaturated nitride deposition. The obtained results are schematically presented in the diagram in Figure 7.

Precipitation of chromium nitrides leads to depletion of the adjacent areas in chromium that had a strong impact on local corrosion resistance. Figure 8 shows the graphs of I_r/I_a values for the base metal and low-temperature region of the HAZ for different heat inputs. Base metal demonstrated the highest density of activation current I_a and the lowest density of reactivation current I_r ($1.83 \cdot 10^{-2}$ and $4.25 \cdot 10^{-6}$, respectively). The degree of activation was the highest at the value of $I_r/I_a = 2.32 \cdot 10^{-4}$. As BM was exposed to a series of thermal cycles, it demonstrated a balanced microstructure. Austenite was uniformly distributed in the ferrite matrix and no harmful secondary phases (such as carbides, nitrides, σ or χ phases) were revealed. This is indicative of the fact that the base metal demonstrated better resistance to local corrosion that did the HAZ metal.

It should be noted that I_r/I_a values gradually increased at dry welding from $2.60 \cdot 10^{-3}$ at minimum heat input (726 J/mm) to $6.67 \cdot 10^{-3}$ at maximum heat input (1383.3 J/mm) (Figure 8). In the latter case, the metal was ex-
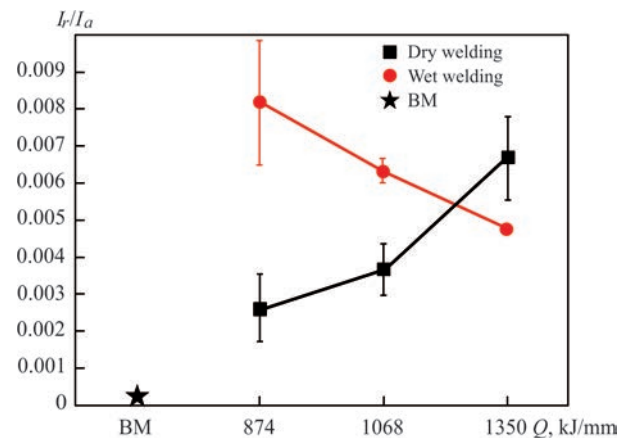

Figure 8. I_r/I_a values for base metal and HAZ low-temperature region for different heat inputs [17]

posed to heat treatment for a longer time and the nitrides also had more time for precipitation on γ/α and α/α boundaries, owing to high coherence. Thus, at dry welding the degree of nitride precipitation and sensitivity to local corrosion increased with heat input increase. At wet welding I_r/I_a values gradually decreased from $8.18 \cdot 10^{-3}$ at minimum heat input to $4.78 \cdot 10^{-3}$ at maximum heat input that is indicative of increase of local corrosion resistance with heat input increase. Dissolution of part of austenite led to higher nitrogen content in ferrite of the HAZ metal. Chromium nitrides were deposited from a ferrite mixture as the high cooling rate led to decrease of

nitrogen solubility. Here, the probability of their deposition decreased, because of the high cooling rate and short ageing time. Thus, at wet welding the volume fraction of chromium nitrides in α-phase decreased with increase of the heat input that promotes lowering of the sensitivity to local corrosion. As a result, the metal of the weld HAZ at wet welding becomes less sensitive to local corrosion at maximum heat input than at dry welding.

Conclusions

1. At present general purpose electrodes and flux-cored wires are used for wet underwater welding of duplex steels, because of absence of specialized welding consumables.

2. Destabilization of the arcing process in the water environment leads to cold cracking in the weld metal. No cracks were revealed in the HAZ.

3. Welds made in air and under the water using coated electrodes, were characterized by a similar structure. Intensive cooling that is ensured by the water environment, did not lead to increase of ferrite content in the weld or HAZ, compared to its content in the joints made in air.

4. Analysis of hardness distribution in the studied joints did not reveal any significant differences in welds made in air and in water. Hardness values, determined in the HAZ, were limited by a range falling between the values of base metal hardness and deposited metal hardness.

5. Size of austenite phases at dry welding was larger than at wet welding under the same heat input conditions. At wet welding the γ/α ratio increased considerably at increase of the heat input: from 27.31 to 39.46 % for the weld center and from 35.01 to 44.9 % for weld metal adjacent to the fusion line.

6. All the studied variants of weld metal composition were insensitive to local corrosion, because of the high PREN values. The weld metal adjacent to the fusion line, showed optimum resistance to local corrosion, and the weld metal demonstrated better local corrosion resistance than did the HAZ. Local corrosion resistance of the HAZ low-temperature zone increased with increase of the heat input at wet welding, while a reverse tendency was observed in the case of dry welding. The HAZ high-temperature zone at dry welding demonstrated an improved local corrosion resistance, compared to that for welded joints made by wet welding under the same heat input conditions.

7. Further studies will be related to stabilization of the arcing process, and determination of the impact of different conditions of the welding process on the possibility of cold crack formation, for instance, effect of water type (fresh, sea), or change of the geometry of welded joint edge preparation and development of specialized electrode materials for wet welding of duplex steels.

1. Charles, J. (2007) Duplex stainless steels, a review after DSS'07 held in Grado. In: *Proc. of the Duplex Stainless Steel Conf.*, *Maastricht. The Netherlands, 18–20 June 2007.*

2. Labanowski, J. Fydrych, D., Rogalski, G., Samson, K. (2011) Underwater welding of duplex stainless steel. *Solid State Phenomena*, **183**, 101–106.

3. Kacar, R. (2004) Effect of solidification mode and morphology of microstructure on the hydrogen content of duplex stainless steel weld metal. *Mater. Design*, 25(**1**), 1–9.

4. Lage, M.A., Assis, K.S., Mattos, O.R. (2015) Hydrogen influence on fracture toughness of the weld metal in super duplex stainless steel (UNS S32750) welded with two different heat input. *Int. J. Hydrogen Energ.*, 40(**47**), 17000–17008.

5. Farrell, J. (1996) *Hyperbaric welding of duplex stainless steel pipelines offshore*: Ph. D. Thesis School of Industrial and Manufacturing Science. Cranfield University.

6. Karlsson, L. (1999) Intermetallic phase precipitation in duplex stainless steels and weld metals metallurgy, influence on properties and welding aspects. *Weld. World*, **43**, 20–41.

7. Labanowski, J. (1997) Duplex steels — new material for chemical processing industry. *Engineering and Chemical Equipment*, **2**, 3–10.

8. Muthupandi, V., Bala Srinivasan, P., Seshadri, S.K., Sundaresan, S. (2003) Effect of weld metal chemistry and heat in put on the structure and properties of duplex stainless steel welds. *Materials Sci. and Eng.*, 358, 9–16.

9. Shinozaki, K., Ke, L., North, T.H. (1992) Hydrogen cracking in duplex stainless steel weld metal. *Welding J.*, **11**, 387–396.

10. Prokop-Strzelczynska, K., Rogalski, G. (2016) Cold cracking susceptibility of joints made of ferritic austenitic duplex steel 2205 during underwater welding. *Biuletyn Instytutu Spawalnictwa w Gliwicach,* 2(**16**), 35–42.

11. Labanowski, J., Prokop-Strzelczynska, K., Rogalski, G., Fydrych, D. (2016) The effect of wet underwater welding on cold cracking susceptibility of duplex stainless steel. *Advances in Materials Sci.*, 16(**2**), 68–77.

12. Kralj, S., Garasic I., Kozuh, Z. (2009) Underwater wet welding of duplex steel. *Welding in the World*, **53**, 35–40.

13. *Yu Hu*, Yonghua SHI, Kun Sun, Xiaoqin Shen (2019) Microstructure evolution and mechanical performance of underwater local dry welded DSS metals at various simulated water depths. *J. of Materials Processing Tech.*, **264**, 366–376.

14. Prokop-Strzelczyńska, K. (2016) Cold cracking susceptibility of joints made of ferriticaustenitic duplex steel 2205 during underwater wet welding. *Biuletyn Instytutu Spawalnictwa w Gliwicach*, 16(**2**), 35–42.

15. Shi, Y., Hu, Y., Li, Z. et al. (2016) Research on porosity of underwater wet FCAW duplex stainless steel. *China Welding*, 25(**2**), 27–33.

16. Shi, Y., Hu, Y., Yi, Y. et al. (2017) Porosity and microstructure of underwater wet FCAW of duplex stainless steel. *Metallography, Microstructure, and Analysis*, **6**, 383–389.

17. *Kun* Sun, Min Zeng, Yonghua SHI et al. (2018) Microstructure and corrosion behavior of S32101 stainless steel underwater dry and wet welded joints. *J. of Materials Processing Technology*, **256**, 190–201.